Galvanic corrosion of gas tungsten arc repair welds in 17-4PH stainless steel in 3·5% NaCl solution

M. R. Tavakoli Shoushtari[1,3], M. H. Moayed[1] and A. Davoodi*[2]

In this paper, the galvanic corrosion of individual components of a 17-4PH repair welded stainless steel in 3·5% NaCl solution was investigated using various dc electrochemical measurements and microscopy. Open circuit potential measurement of the regions in the vicinity of a repair weld [i.e. parent metal, weld metal and heat affected zone (HAZ)] in 17-4PH stainless steel in 3·5% NaCl solution indicated that the most likely galvanic couple was between HAZ and weld with the HAZ acting as the anode and weld metal as the cathode. Slow scan rate potentiodynamic polarisation measurement of pitting potentials revealed a lower passive current density and a higher pitting potential in the weld region, while the HAZ showed the highest passive current density and the lowest pitting potential. Observation of the material after applying an anodic potential close to the pitting potential of the individual weld parts also confirmed the formation of several stable pits in the HAZ but only a few metastable pits in the weld and parent metal zones. Galvanic coupling using a zero resistance ammeter also showed a higher current density in the weld metal/HAZ as compared with the parent metal/HAZ and parent metal/weld galvanic couples. Although, the current densities in all measurements were in the range of a few to tenths of nanoampere per square centimetre, it can still be concluded that the weld metal/HAZ couple has the highest risk of galvanic corrosion among the three individual galvanic couples.

Keywords: GTA welding, 17-4PH stainless steel, Galvanic corrosion, Potentiodynamic polarisation, ZRA measurement

Introduction

Application of precipitation hardened stainless steels has become progressively more important where their special properties can be utilised.[1,2] The most important of these properties are easy fabrication, high strength, relatively good ductility and good corrosion resistance.[1–5] The 17-4PH (AISI type 630 or UNS S17400) stainless steel from this family is a martensitic stainless steel containing approximately 3–5 wt-%Cu and is strengthened by the precipitation of highly dispersed copper enriched zones inside the temper lath martensitic matrix; this has low carbon content and is stable at room temperature.[3–6] The formation of a small volume fraction of delta ferrite has also been reported.[6,7] Use of this alloy has increased for a variety of applications, particularly in marine construction, chemical industry and power plant, due to their excellent combination of mechanical properties comparable to type 304 austenitic stainless steel and corrosion and oxidation resistance comparable to type 410 martensitic stainless steel.[8,9] The alloy can be easily machined in solution treated condition with fast cooling with relatively low hardness. After machining operations, it can be hardened for a wide range of mechanical properties and hardness by the precipitation aging heat treatment at temperatures between 480 and 620°C. The increase in hardness and strength is due to the precipitation hardening that occurs over the martensite structure previously formed during the solution treatment.[4]

To utilise these properties, various joining techniques, in particular welding processes such as gas tungsten arc welding (GTAW) are commonly used. In other words, welding processes are indispensable for the development of almost all manufactured product.[10] Since producing this type of stainless steel is more expensive than other types,[11] in the presence of any defects and cracks, replacement of exactly the same material is costly. In this circumstance, repair welding is a common technique to reduce both shutdown periods and the replacement costs for new components. Nevertheless, solidification processes, such as welding, alter the microstructure and composition of the alloy in the weld zone. It also induces microstructural variations in heat affected zone (HAZ) due to the heat input induced by welding operation.[10–12]

[1]Metallurgical and Materials Engineering Department, Faculty of Engineering, Ferdowsi University of Mashhad, Mashhad 91775-11, Iran
[2]Materials Engineering Department, Faculty of Engineering, Sabzevar Tarbiat Moallem University, Sabzevar 397, Iran
[3]Materials Engineering Department, Faculty of Engineering, Shahid Chamran University, Ahvaz 61355, Iran

*Corresponding author, email adavoodi@kth.se

Published by Maney on behalf of the Institute
Received 28 December 2008; accepted 13 April 2009
DOI 10.1179/174327809X419221

The microstructure of the weld pool in 17-4PH mainly contains martensite, but a small fraction of delta ferrite and untempered martensite is also observed.[10]

The microstructural changes in the weld areas not only change the mechanical properties but also may cause electrochemical dissimilarity of the individual parts in the weldment. Therefore, as a result of microstructural and compositional changes in the HAZ, galvanic corrosion may occur in different parts of a welded specimen.[10–12] Consequently, galvanic corrosion cannot be disregarded due to galvanic pair between weld zone and adjacent HAZ and base metal region when exposed to corrosive environments.

Recently, Kumar and Srinivasan[13] reported the influence of GTAW on the microstructure, hardness and corrosion behaviour of 410 martensitic stainless steel in various concentrations of sodium chloride electrolyte. Similarity in general corrosion resistance and passivation behaviour of the base metal, weld metal and HAZ regions were obtained in chloride test electrolytes; however, in terms of pitting corrosion resistance, the martensitic structured weld and HAZ region showed much lower pitting resistance compared to the base region. They concluded that the microstructural variations due to welding did not influence significantly the general corrosion and passivation behaviour but have a marginal adverse influence on the pitting corrosion resistance.[13]

Regarding the corrosion behaviour of welded 17-4PH stainless steel, Nowacki stated that shielded metal arc welding and flux core arc welding using covered Avesta 309 Mo and core wire Cvomacore DW309 MoL weld filler materials provide very good corrosion resistance in 50% HNO_3 solution. He also observed that the corrosion that developed in HAZ mainly had a pitting character, while the welds had an excellent resistance.[12] To investigate the galvanic corrosion among different parts of weldment, sample preparation of working electrode plays an important role. Garcia *et al.*[14] employed a small scale mini-electrochemical cell to investigate the pitting corrosion and galvanic behaviour of different parts of a weldment. Kwok *et al.*[15] used a working electrode containing a whole welded specimen coupled to unwelded one to measure galvanic current. Since most reports that have been published on galvanic corrosion are based on measurements between unwelded and welded specimens rather than samples prepared from individual parts of welded specimen, the interpretation of the measured currents is difficult.

This work is aimed to investigate the galvanic corrosion among possible galvanic couples: weld/base and HAZ/base and weld/HAZ in repair welded 17-4PH stainless steel by utilising microscopic studies, measurement of the corrosion potential of the three individual zones, determination of the pitting parameters and passivity current by potentiodynamic polarisation measurements. In order to accomplish this, the individual parts of a welded specimen were extracted and coupled together. Galvanic potential and current densities were measured by employing zero resistance ammeter (ZRA) technique in 3·5 wt-% NaCl solution.

Materials and experimental methods

A 17-4PH stainless steel bar with dimensions of 93 mm in diameter and 400 mm in length was used. The

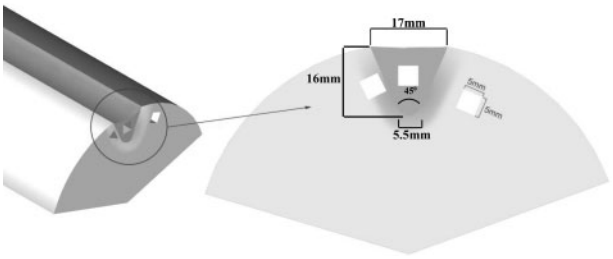

1 Schematic drawing of weldment dimensions and individual sample extracted from base, HAZ and weld regions used in this study

samples were delivered in the following condition: solution treated at 1040°C for 1 h and oil quenched. For precipitation hardening, the sample was heat treated at 550°C for 4 h and then air cooled. The precipitation hardening cycle was repeated by heating the sample up 620°C for 4 h and then air cooled. The chemical analysis of sample was obtained by spark optical emission spectroscopy. Assuming the presence of metallurgical defects in the specimen, a repair welding procedure was performed to simulate the practical conditions. For this purpose, first, the sound sample was cut by slab milling, and then the prepared gap was filled by the welding process as shown in Fig. 1. According to the standard American Society of Mechanical Engineers section 2, the GTAW operation used a standard (ER630) filler electrode. The welding parameters were as follows: current, 130–150 A; voltage, 14–16 V; welding speed and 180–200 mm min^{-1}. Argon with purity of 99·999% with 11–14 L min^{-1} flow rate was used as protective gas.

The samples were hot mounted, then ground from 60 to 1200 SiC papers before finishing using 1 μm diamond paste. To determine the weld area and HAZ, the sample was exposed to Marble's reagent (4 g $CuSO_4$, 20 mL HCl and 20 mL distilled water) for macroetch optical examination. To identify the microstructure constituents in weldment, the cross-section of the samples was placed in Vilella's reagent (1 g picric acid, 100 mL ethyl alcohol and 5 mL hydrochloric acid). Metallographic examination was carried out using Olympus BX60M optical microscope. Scanning electron microscopy samples used for analysis of base alloy and HAZ and the weld metal were the same as samples prepared for metallographic examination. Scanning electron micrographs were taken using a Leo1455VP SEM with 15 kV accelerating voltage. Hardness test, HRC, was performed using an Avery-Denison instrument in the three regions (i.e. weld, base and HAZ), with five measurement points in each area. For corrosion studies, identical samples of base, weld and HAZ regions were obtained as shown schematically in Fig. 1, in which the cross-section area was 5×5 mm for each component. Before corrosion tests, the samples were degreased in 10% NaOH for 1 min at 50–60°C, washed by distilled water and dried. In the next step, the samples were ultrasonically cleaned in acetone for 2 min in room temperature. To avoid crevice corrosion at the gap between the specimen and mounting material during the corrosion tests, the interface between sample and mounting material was covered by lacquer.[14]

An ACM Instruments electrochemical workstation was employed for the electrochemical tests with a

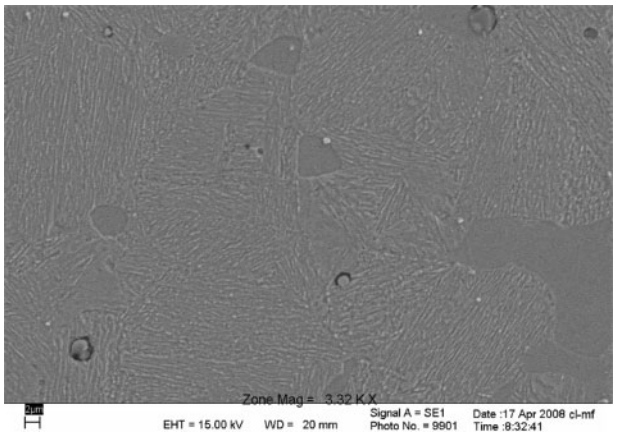

2 Image (SEM) of microstructure of as received 17-4PH stainless steel containing alpha ferrite phase with white lamellar in shape and lath tempered martensite as matrix

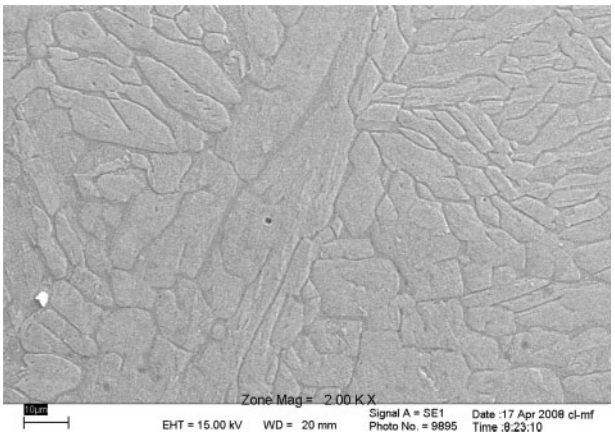

3 Image (SEM) of microstructure of weld region in GTAW of 17-4PH showing untempered martensite

saturated calomel reference electrode (SCE) and platinum wire counter electrode with a surface of 2 cm^2. All tests related to pitting and galvanic corrosion were carried out in 3·5 wt-% NaCl solution at ambient temperature (22–25°C). First, the rest potential was measured, i.e. each sample was placed inside the solution for 1 h, and the changes in its corrosion potential were recorded. Each test was repeated three times to ensure reproducibility, and average values were reported as rest potential. To obtain the polarisation curve, each sample was immersed inside the solution for 1 h before the test for stabilisation of its rest potential. Potentiodynamic polarisation was carried out with a scan rate of 3 mV min^{-1} over a range of 200 mV cathodic potential, offset to the rest potential, up to the potential value in where the sudden current increasing occurred due to extensive pitting corrosion. After anodic polarisation close to pitting potential, the samples were ultrasonically cleaned then washed with alcohol, dried, then etched by Vilella's reagent. In this way, the stable and metastable pitting morphologies were observed by SEM. Moreover, passivity behaviour was evaluated by potentiostatic polarisation of individual base, HAZ and weld zones at an anodic potential of 150 mV(SCE). The aim was to examine the resistance to pitting corrosion in samples within the passivity zone.

Finally, coupled potential and current density measurements of the possible galvanic cells between the weld/base, HAZ/base and weld/HAZ were carried out using a ZRA during 1 and 42 h. During short term measurement of 42 h, 10 min data points have been collected in every 6 h.

Results and discussion

Chemical analysis and microstructure evaluation

The chemical analysis of the stainless steel alloy was Fe–0·01C–0·86Mn–0·021P–0·007S–0·8Si–15·74Cr–3·96Ni–0·06Mo–2·74Cu–0·3(Nb+V) (wt-%). The chemical composition of the alloy is in agreement with the 17-4PH stainless steel according to the ASTM A705 (grade 630) standard for precipitation hardening forged stainless steel.[16] According to the delivery conditions of this alloy, as described in the section on 'Materials and experimental methods', the performed heat treatment leads to the achievement of required mechanical properties, including tensile strength, elongation and hardness. Furthermore, as a result of heat treatment, the microstructure of as received sample contains temper lath martensite and ferrite as shown in Fig. 2. When solidification occurs as primary ferrite, some austenite forms at the ferrite cell and dendrite boundaries due to a peritectic–eutectic reaction at the end of solidification. After quenching in oil and transforming austenite to the martensite, the microstructure consists of primary ferrite dendrites with an interlayer of martensite.[11] After the tempering stage, the microstructure then consists of recrystallised α-ferrite phase (appeared as white lamellar layer in Fig. 2) formed in the tempered martensite. The presence of nano size Cu rich phase precipitates is also expected during the aging treatment, and this has been previously reported by others.[5]

Different regions induced by the GTAW operation were first distinguished by employing a macroetch examination. The SEM image of the weld zone of 17-4PH is also presented in Fig. 3. The structure includes coarse and untempered lath martensite surrounded by strings of delta ferrite. The result is presented in Fig. 4, which shows the base metal, HAZ, fusion line and weld metal zones. According to the macroetch test, the size of the HAZ can be estimated to be $\sim$3 mm. A series of microstructures from near the weld metal region (which shows untempered lath martensite, delta ferrite and coarse grains) to near the base metal region (containing fine grains and overaged martensite) is shown (Fig. 4). Based on metallographic observations, the HAZ can be split to the four subregions from weld region towards the base area. Figure 4*a* represents the microstructure of the weld zone containing multidirectional martensite laths, which has been shown previously in more detail in Fig. 3. Figure 4*b* shows the portion of the HAZ adjacent to the fusion boundary. This is a solution treated region, in which precipitates are re-dissolved and the bulk of the microstructure at elevated temperature consists of delta ferrite, but some austenite may be present at the ferrite grain boundaries. Upon cooling to room temperature, the microstructure includes lath martensite, and some of the ferrite remained in the microstructure. The presence of ferrite can promote local softening relative to the adjacent fusion zone and HAZ. In Fig. 4*c*, the microstructure will be delta ferrite and austenite at elevated

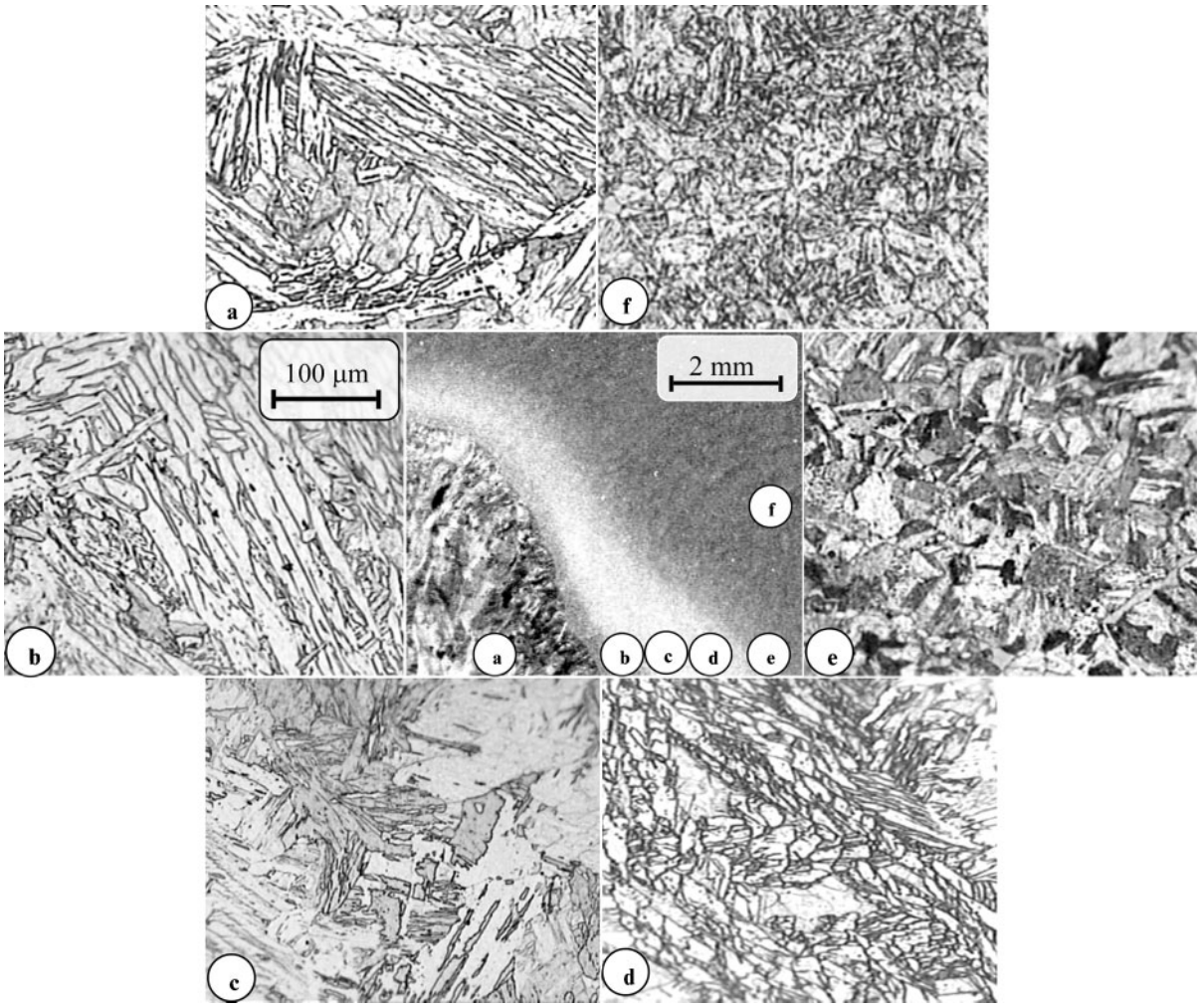

4 Macrography examination of weldment showing *a* weld region, *b–e* HAZ subregions and *f* base region: macroetchant, Marble's reagent (4 g $CuSO_4$, 20 mL HCl and 20 mL distilled water); all optical images' magnification is the same, shown in *b*

temperature. The temperatures in this region of the HAZ are sufficiently high that austenite grain growth will occur. Upon cooling, this region will be transformed to coarse martensite and with some delta ferrite. Figure 4*d*, is an image of the section that was heated into the two-phase region (delta ferrite plus austenite during welding), but because the temperature is lower than in region c, grain growth will not be so pronounced. In Fig. 4*e*, the microstructure appears virtually identical to the overaged base metal, resulting in some local softening relative to the base metal. These structural variations in the HAZ have also been reported in martensitic stainless steel.[11,17] Finally, the base metal area which contains tempered lath martensite and ferrite is shown in Fig. 4*f* and similar to Fig. 2 in agreement with the literature.[1]

Gas tungsten arc welding process also induces variations in the mechanical properties of the individual regions. As an example, hardness measurements along the base, HAZ and weld regions are shown in Fig. 5 and reveal that the hardness decreases in the weld and HAZ regions. This can be attributed to the lack of Cu rich phase precipitates and softening phenomena in weld and HAZ respectively.[11]

In summary, the GTA welding operation induces microstructural changes and, consequently, mechanical behaviour among base, HAZ and weld regions. Influences of welding on corrosion behaviour are shown in following sections.

Open circuit potential, potentiodynamic and potentiostatic measurements

Variations in the open circuit potential (OCP) of the base alloy, HAZ, and weld zone of 17-4PH stainless steel

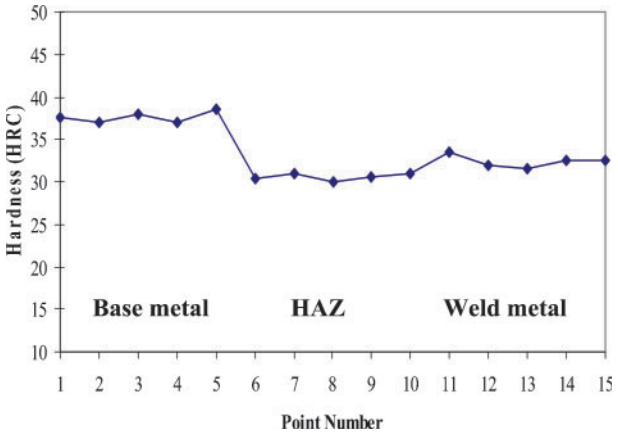

5 Hardness profile measure along base, HAZ and weld region in repair welded 17-4PH stainless steel

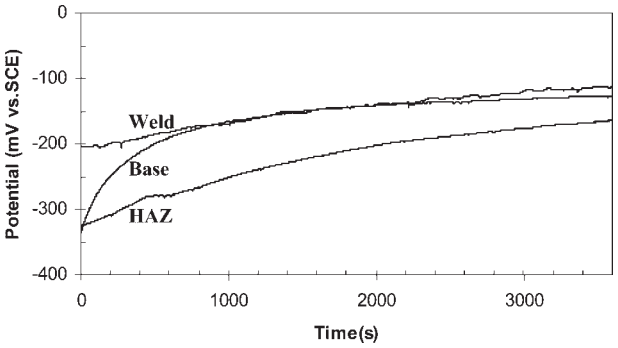

6 Variation of OCP for individual base, HAZ and weld regions of repair welded 17-4PH stainless steel immersed for 1 h in 3·5% NaCl solution

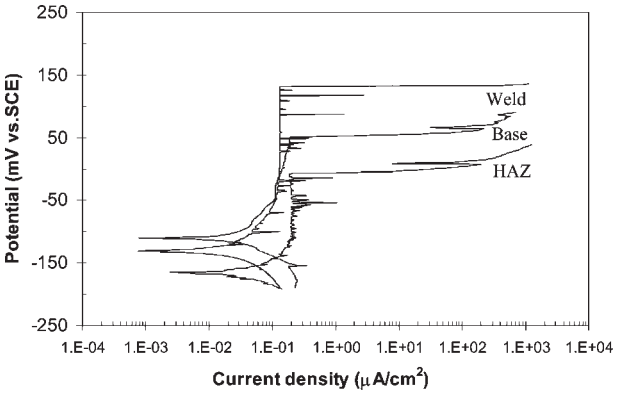

7 Potentiodynamic polarisation curve for individual base, HAZ and weld regions of repair welded 17-4PH stainless steel immersed in 3·5% NaCl solution: scan rate was 3 mV min^{-1}

immersed in 3·5% NaCl solution were monitored, and the results are presented in Fig. 6. As can be seen, the corrosion potential associated with base metal and HAZ and weld all show a gradual increase with time, which is more enhanced in base region; this is evidence for the development of the passive layers. All three regions almost reach the steady state after 1 h exposure in 3·5% NaCl solution, and the corrosion potentials for weld, base and HAZ zones are about −110, −130 and −165 mV(SCE) respectively. Therefore, measuring the corrosion potential demonstrate that the potential of weld region is more positive than the HAZ, while the corrosion potential of the base metal is situated between the weld and HAZ regions. This can be attributed, for example, to the improved integrity of passive film on weld surface in compared with the HAZ. In contrast, the HAZ has the lowest corrosion potential, ∼35 mV less than the base metal, which indicates that the microstructural changes in the HAZ reduce its passivity. The OCP difference among the three possible galvanic corrosion couples, which is defined as the driving force for possible galvanic corrosion, demonstrates that the most dangerous couple is likely to be associated with the weld/HAZ couple followed by base HAZ and weld base couples. However, the OCP difference between the weld and HAZ gradually decreases from about 120 mV in the beginning to an almost constant value of ∼55 mV after 1 h exposure. On the other hand, the OCP difference between the base and HAZ seems to increase within the exposure time, reaching a ∼35 mV difference.

The potentiodynamic polarisation curves for the individual base alloy, HAZ and weld zone components of the 17-4PH SS weld are shown in Fig. 7. It is evident that the weld metal again has the highest OCP value, while the OCP of the base metal is close to the weld zone, which is in agreement with Fig. 6. Moreover, the corrosion rate calculated by Tafel extrapolation reveals that weld and base regions have more or less similar values, while the corrosion rate of HAZ is several times that of the base and weld regions.

The results of pitting potential (breakdown potential) for all three zones of the 17-4PH stainless steel weld show that the pitting potential of HAZ, base metal and weld metal are about −7, +50 and +130 mV(SCE) respectively. This is an indication of a lower pitting corrosion resistance for the HAZ compared to the base and weld zones. While the GTAW operation increases extensively the passivity domain in the weld region (and this is favourable), it appears to decrease the passivity domain in the HAZ, as can be seen in Fig. 7. Moreover, the average passivity current density calculated from Fig. 7 for the three zones reveals a current density of 0·2, 0·13 and 0·13 μA cm^{-2} for HAZ, base and weld zones respectively. Therefore, potentiodynamic measurements of the weldment confirm that the HAZ shows slightly poor passivation behaviour with ∼70% higher passive current density than the base and weld metals. Although the passive current of base and weld zones seems to be similar, it is clear that this value for base region gradually increased from 0·05 to 0·23 μA cm^{-2} in the passivity domain, while it remains almost constant (0·13 μA cm^{-2}) for the weld region as shown in Fig. 7.

By utilising a very slow scan rate (3 mV min^{-1}), the existence of metastable pits could be also exhibited as current fluctuations in passivity range (Fig. 7) for all base, HAZ and weld zones. In the passivity potential domain of HAZ (from its OCP to breakdown potential), the number of current peaks in HAZ is much more than the weld and base regions, which is indeed an indication of lower pitting resistance associated to the HAZ in comparison to the other area.

In order to observe the morphology of pits, anodic polarisation of the individual weld components was carried out close to their pitting potential. Formation of several stable pits in HAZ specimen revealed the inferior pitting resistance of this region compared to the weld zone and base alloy. While during similar polarisation test on the base alloy and weld zone, only several metastable pits were detected. Figure 8*a* and *b* illustrates the metastable pit morphology in which it seems that surface inclusions play the major role initiation sites. The morphology of stable pits formed in HAZ regions shows lacy covers over the pits containing several micropores with a network character (Fig. 8). This stable pit shape in stainless steels has been also reported by others.[18]

Figure 9 shows the passive current density variations with time for the weld zone, HAZ and base alloy of 17-4PH stainless steel after applying an anodic potential of 150 mV with respect to the rest potential in a 3·5 wt-% NaCl solution at ambient temperature. In this case, all three zones lie within the passivity state with initial stable current densities ∼0·5 μA cm^{-2}. The current densities associated with base, HAZ and weld zones decrease with time (and faster in the weld zone). This is

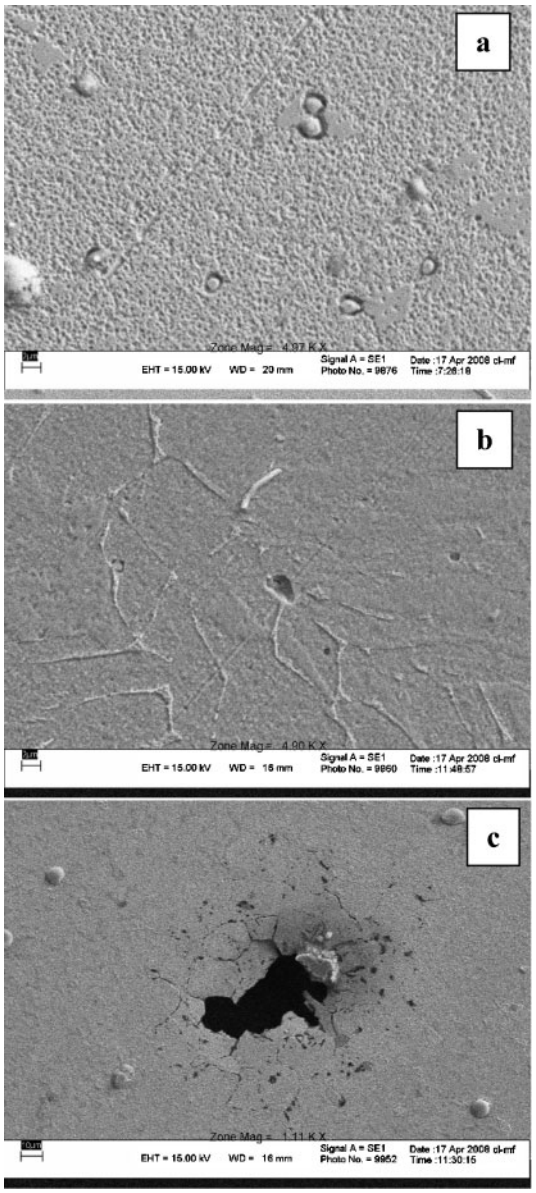

8 Images (SEM) of pitting morphology observed in *a* base, *b* weld and *c* HAZ zones after anodic polarisation close to pitting potential shown in Fig. 7

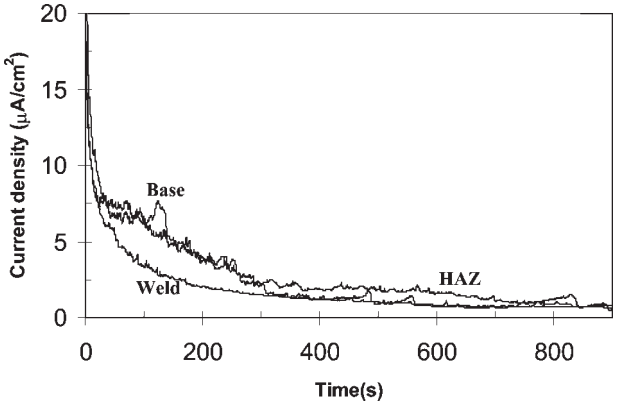

9 Potentiostatic curve for individual base, HAZ and weld regions of repair welded 17-4PH stainless steel in 3·5% NaCl solution during 900 s: anodic potential was 150 mV offset to rest potential

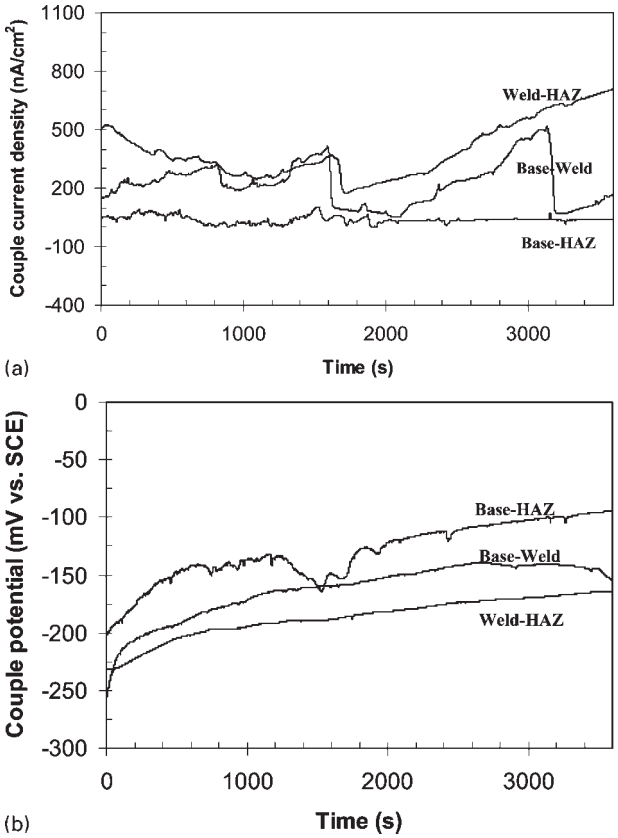

10 *a* galvanic couple current density and *b* couple potential of three couples during 1 h exposure time in 3·5% NaCl solution measured by ZRA method

again an indication of more or less similar passivation behaviour for all three zones, which confirms the previous potentiodynamic measurements in Fig. 7. However, the irregular current density fluctuations observed on potentiostatic polarisation at 150 mV(SCE) anodic applied potential for base and HAZ are related to the formation of unstable pits.

Zero resistance ammeter measurements

Galvanic current densities were measured using the ZRA method for the galvanic couples of base/weld, base/HAZ and HAZ/weld for 1 and 42 h (with 6 h interval data acquisition measurement) of exposure time. The result of the galvanic current density and couple potential for the 1 h experiment is presented in Fig. 10. Generally, the galvanic current density of base/HAZ couple is a minimum compared with the other couples where the average current is $\sim$40 nA cm^{-2} with fluctuations up to 150 nA cm^{-2} also observed during 1 h exposure time (Fig. 10*a*). The potential variations of the cell over 1 h are presented in (Fig. 10*b*); the gradual increase in galvanic potential from -200 to -95 mV(SCE) is attributed to an effectively equal positive shift of both anode and cathode OCPs (since the couple current is almost constant), and it indicates the consistency and continuity of passivity on both electrodes. The current measured by ZRA in base/HAZ couple can be mainly associated to the anodic reaction on HAZ surface area, which is equal to the cathodic reaction on the base zone. It should be noticed that the generated net anodic current by anode, HAZ, is associated with the passive current density and the

collected net cathodic current on cathode, weld, related to the oxygen reduction reaction.

A considerably higher galvanic current density was measured for the base/weld couple with an average value of 224 nA cm^{-2} with uneven distribution from a minimum value of 70 to a maximum of 500 nA cm^{-2}, as seen in Fig. 10*a*. Taking into account the couple potential variations in Fig. 10*b*, again, a gradual increase in couple galvanic potential from −250 to −150 mV(SCE) is observed, which is an indication of almost equal positive shift of anode and cathode OCPs (since the couple current is more or less constant). Therefore, the current measured by ZRA in base/weld couple can be mainly associated to cathodic reaction on the weld zone, which is equal to the anodic reaction on base surface area. Interestingly, notice that in contrast with the previous couple, here, the base region plays an opposite role.

Regarding the third galvanic couple, weld/HAZ, the highest current density was measured with an average value of 400 nA cm^{-2} with a maximum of 700 nA cm^{-2}, as seen in Fig. 10*a*. The couple galvanic potential slowly increases from −230 to −165 mV(SCE) which is an almost equal positive shift of anode and cathode OCPs. Therefore, the current measured in the weld/HAZ couple can be mainly associated to the cathodic reaction on the weld zone, which is equal to the anodic reaction on HAZ surface area.

Three possible galvanic cells including base/weld, base/HAZ and HAZ/weld can be created. Based on corrosion potential difference between cathode and anode of the mentioned cells, in all cells, the weld and HAZ regions act as cathode and anode respectively. It should be emphasised that, in all three galvanic couples, the anode is polarised just into the passive region; therefore, the anodic current is associated with the passive current.

In summary, ZRA measurements for 1 h exposure indicate a significantly larger current density in the weld/HAZ pair compared to the other two. However, it seems that this short time measurement may not be sufficient to exactly discriminate the different behaviour of possible galvanic corrosion, and previously described judgment based on the above results should not be extrapolated for a longer time. Therefore, the galvanic corrosion measurements were repeated over a longer 42 h time period, and these data are presented in Fig. 11.

The results reveal that during 42 h immersion of 17-4PH in 3·5% NaCl solution, while the current density slowly increases from about 32 to 66 nA cm^{-2} in the HAZ/weld couple (Fig. 11*a*), the corresponding couple potential decreases from −70 to −100 mV(SCE) (Fig. 11*b*). Decreasing in couple potential and simultaneously increasing in galvanic current density may be an indication of possible depolarisation of anode, here HAZ, rather than depolarisation of cathode or due to reducing nobleness of HAZ, which in turn leads to increasing in current density. A slight decrease in current density, ~10 nA cm^{-2}, during the last 6 h exposure time was also observed; however, the couple potential eventually reaches a stable value around −100 mV(SCE), which means that an equilibrium condition has been achieved between the cathode and anode of cell. Similar methods were performed to collect the data for two other

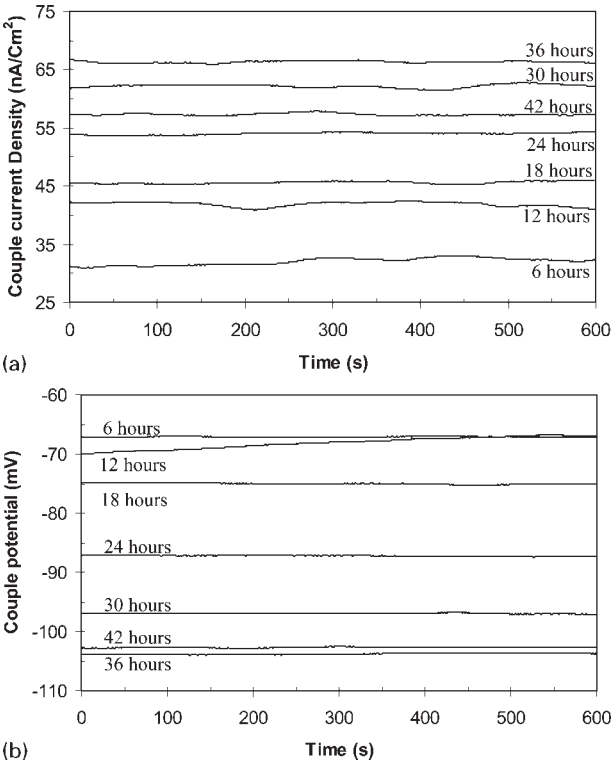

11 ***a*** **galvanic couple current density and** ***b*** **couple potential data acquisition of weld/HAZ cell: data have been collected for 10 min in 6 h intervals up to 42 h exposure time in 3·5% NaCl solution**

couples and to simplify the interpretation; the average values of each 10 min data for 6 h intervals are shown in Fig. 12. As can be seen, after an initial transient, significantly lower current densities are observed for the weld/base and base/HAZ couples. Up to 18 h, the base/weld pair shows the lowest current density (<1 nA cm^{-2}), whereas after this time, the base/HAZ couple shows the minimum value (Fig. 12*a*). Both couple potentials increase from around −200 to −7 mV(SCE) and from −185 to −62 mV(SCE) in weld/base and HAZ/base respectively, as shown in Fig. 12*b*. These observations show clearly the establishment and improvement of passivity on both electrodes with immersion time.

Moreover, while the current density of the base/HAZ couple remains almost constant below 1 to 2 nA cm^{-2}, it gradually increases up to 7 nA cm^{-2} for the base/weld pair (Fig. 12*a*). This means that, although the driving force, OCP differences after the first hour of exposure in base/weld couple is less than the base/HAZ value (Fig. 6), but after 42 h, the OCP difference in base/weld couple becomes greater than the base/HAZ.

In summary, from galvanic corrosion point of view and based on the results obtained by ZRA galvanic coupling, in GTA repair weldment in 17-4PH stainless steel in 3·5% NaCl solution, current densities of a few to tenths of nanoampere per square centimetre were detected. It can be also concluded that the weld/HAZ couple has the highest driving force for galvanic corrosion with the consequent highest risk among the three individual galvanic couples for corrosion as an anode. The results also reveal that two other possible galvanic cells, base/HAZ and base/weld couples, are almost harmless with negligible galvanic current of few nanoampere per square centimetre. It should be

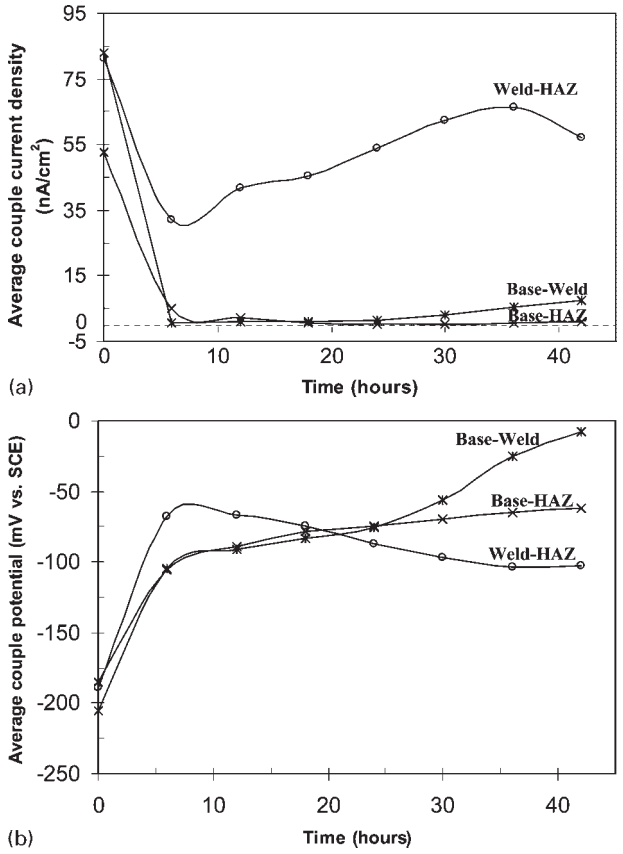

12 ***a*** **average galvanic couple current density and** ***b*** **average couple potential of three galvanic couples during 42 h exposure time in 3·5% NaCl solution: average values of data for 10 min measurements were used**

mentioned that, in ZRA measurement, equal surface area of base, HAZ and weld were used. However, in practice, when a piece of 17-4PH stainless steel is welded, the surface area related to the weld, and particularly, HAZ zones are much smaller than the base metal. Since the HAZ acts as an anode in the galvanic couples, therefore, due to the kinetic effect of smaller anode/cathode surface area ratio, in practical situations, galvanic corrosion of the HAZ might be expected to be greater than that observed in this work. First, the HAZ is corroded, and consequently, another galvanic cell is shaped between weld region as cathode and base metal as anode. Although in simultaneous formation, all three cells cannot be ignored, the highest possible galvanic cell current is associated with the weld/HAZ cell.

The overall current density measured by the ZRA method in galvanic pairs can be attributed to the microstructure differences among three individual regions and can be divided into specific currents attributed to the local cathodes and anodes on the surface. The weld operation induces microstructure changes in weld and HAZ zones and has no effect on base alloy region. The weld zone contains major untempered martensite laths with a variable amount of ferrite (Fig. 3), whereas HAZ has completely different microstructure containing a spectrum of constituents from coarse and fine grain untempered martensite to overaged martensite with different delta ferrite volume fractions. In addition, the amount of delta ferrite is likely to be different in the weld zone compared to the two other regions. It seems that these two differences, the type of martensite and amount of ferrite, play the crucial role in galvanic corrosion.

First, assume the formation of a galvanic cell comprising a weld as cathode and HAZ as the anode of the cell. In this cell, on the weld zone, the cathodic current reaction is more feasible (comparing the cathodic branch of weld and HAZ regions in polarisation curve, as shown in Fig. 7) and predominantly is due to the oxygen reduction reaction current on the weld surface constituents (although it is not clear that how much cathodic reaction current can be associated to the martensite and/or ferrite). During galvanic coupling of the weld metal to the HAZ, the anodic reaction in the weld zone is very small and mainly can be attributed to the passive current. On the other hand, on the anode component (i.e. the HAZ), the anodic current reaction is more feasible (comparing the anodic branch of weld and HAZ regions in polarisation curve, as shown in Fig. 7) and predominantly is associated with the passive current of the surface constituents including martensite and ferrite. Although anodic polarisation of the HAZ, when it is coupled to the weld metal, may cause pitting corrosion in the longer term. However, distinguishing the fraction of anodic current associated to passivity and pitting is not straightforward. Obviously, during galvanic coupling of the HAZ to the weld, a very small amount of oxygen reduction as cathodic reaction in HAZ also occurs. In summary, the overall current measured by the ZRA method is exactly the net current associated with the HAZ as anode that flows toward the weld as cathode as shown in Figs. 11 and 12.

A similar approach can be used to address the formation of the other galvanic cells. Considering the measured galvanic current of the three possible cells (Fig. 12), revealing the highest current density for the weld/HAZ cell, the difference in measured current can be related to the existing cell driving force and, by extension, the difference in microstructure between the cell anode and cathode. From the cell driving force point of view, the corrosion potential difference between weld and HAZ is bigger than that between two others (Fig. 6). Therefore, the galvanic current associated with the weld/HAZ cell has the greatest value. Owing to different martensite structure and probably higher portion of ferrite in the HAZ compared to the weld region, the overall anodic current in HAZ is higher than the weld and consequently higher than the two other galvanic couples. As it was mentioned before, although the couple current between base and HAZ is less than that between weld and HAZ, as can be seen in Fig. 12, in reality, due to greater kinetic effect of anode/cathode surface area ratio, it cannot be completely ignored. Moreover, it seems that more investigations on the details of the 17-4PH stainless steel microstructure influence on galvanic and localised corrosion, particularly in determining the corrosion initiation sites and the effect of nanosize Cu rich precipitates with more accurate techniques such as TEM, are certainly needed. It should be noted also that microsegregation can also have an influence on initiation of corrosion, as was pointed out in previous reports.[19,20] Although this phenomenon was observed in other stainless steel grades, particularly in irradiated specimens, in 17-4PH, in the present study, microsegregation phenomena at least was not detectable.

It should be finally pointed out that, based on the galvanic current measurements in the range of few nanoampere per square centimetre after 42 h exposure in an aggressive solution of 3·5% NaCl by ZRA, a proper repair welding operation on 17-4PH stainless steel is indicated. However, the measured couple current is the average value on the whole sample surface area and may underestimate the galvanic current sustainable due to galvanic couple and not measure the local currents generated by individual constituents. In other words, the actual currents at the microscopic level may be much greater than the values measured by ZRA for the same area, as it has been reported elsewhere, by employing local probe methods such as the scanning reference electrode technique.[21] Therefore, although the galvanic current measured here by ZRA was not high in absolute terms, by generation of such currents, the formation of stable pits in HAZ can be predicted after long term exposure. Furthermore, to eliminate the destructive influence of HAZ formation, proper heat treatment including solution annealing followed by an aging heat treatment can be suggested. Such work is being planned, and the results are presented elsewhere.[22]

Conclusion

The aim of this work was to study the galvanic corrosion between individual components of a 17-4PH repair welded stainless steel in 3·5% NaCl solution using various dc electrochemical measurements. The results can be summarised as follows.

1. Regardless of any effect on mechanical properties, from a corrosion point of view, gas tungsten arc weld repairing of 17-4PH stainless steel using ER630 filler metal and following described welding procedure was satisfactory. The current densities in all measurements were in the range of a few to tenths of nanoampere per square centimetre, indicating sustainability of passivity as a result of proper welding procedure.

2. Measurement of the OCPs of individual components of the weldment in 17-4PH stainless steel in 3·5% NaCl solution revealed corrosion potentials for the weld metal, base metal and HAZ that were about −110, −130 and −165 mV(SCE) respectively, indicating a possible formation of a galvanic couple between the HAZ and weld, with the HAZ as anode and weld metal as cathode.

3. Slow scan rate potentiodynamic polarisation measurement of the pitting potential revealed a lower passive current density and highest pitting potential in the weld region, while the HAZ showed the highest passive current density and the lowest pitting potential. Microscopic observation after anodic polarisation close to the pitting potential also confirmed the formation of several stable pits in the HAZ region, but only a few small metastable pits were detected in the weld and base zones.

4. Short term measurement (1 h) of the galvanic couples between equal surface areas of HAZ and weld zone revealed significantly higher current densities in comparison to the base/HAZ and base/weld galvanic couples. The average current densities of 40, 224 and 400 nA cm^{-2} were measured for galvanic couple of base/HAZ, base/weld and weld/HAZ respectively.

5. Long term (42 h) galvanic current measurements also showed a higher current density in the weld/HAZ couple compared to the base/HAZ and base/weld galvanic couples. Therefore, the weld/HAZ couple is confirmed to have the highest risk among the three possible galvanic couples in a weld repair on 17-4PH stainless steel.

Acknowledgement

Authors would like to appreciate the financial support from Ferdowsi University of Mashhad through the provision of laboratory facilities during the period that this research was conducted. Authors also would like to acknowledge Dr K. Ranjbar in Shahid Chamran University of Ahvaz for assisting on SEM examination.

References

1. J. R. Davis: 'ASM specialty handbook stainless steel', 34; 1994, Materials Park, OH, ASM International.
2. C. N. Hsiao, C. S. Chiou and J. R. Yong: *Mater. Chem. Phys.*, 2002, **74**, 132–142.
3. W. Jun, Z. Hong, L. Cong, Q. Shao-Yu and S. Bao-Luo: *Mater. Charact.*, 2006, **57**, 274–280.
4. J. D. Bressan, D. P. Daros, A. Sokolowski, R. A. Mesquita and C. A. Barbosa: *J. Mater. Process. Technol.*, 2008, **205**, 353–359.
5. J. H. Wu and C. K. Lin: *J. Mater. Sci.*, 2003, **38**, 965–971.
6. M. Murayama, Y. Katayama and K. Hono: *Metall. Mater. Trans. A.*, 1999, **30A**, 345–353.
7. W. C. Chiang, C. C. Pu, B. L. Yu and J. K. Wu: *Mater. Lett.*, 2003, **57**, 2485–2488.
8. '17-4PH stainless steel product data bulletin'; 2000, Middleton, AK Steel Corp.
9. A. U. Malik, N. A. Siddiqi and I. N. Andijani: *Desalination*, 1994, **97**, 189–197.
10. in 'ASM handbook', 10th edn, Vol. 6, 'Welding, brazing, and soldering', 482–490; 1993, Materials Park, OH, ASM International.
11. J. C. Lippold and D. J. Kotecki: 'Welding metallurgy and weldability of stainless steel', 264–286; 2005, New York, John Wiley & Sons.
12. J. Nowacki: *J. Mater. Process. Technol.*, 2004, **157–158**, 578–583.
13. M. P. S. Kumar and P. B. Srinivasan: *Mater. Lett.*, 2008, **62**, 2887–2890.
14. C. Garcia, F. Martin, P. de Tiedra, Y. Blanco and M. Lopez: *Corros. Sci.*, 2008, **50**, 1184–1194.
15. C. T. Kwok, S. L. Fong, F. T. Cheng and H. C. Man: *J. Mater. Process. Technol.*, 2006, **176**, 168–178.
16. 'Standard specification for age-hardening stainless steel forgings', ASTM A 705, ASTM, Philadelphia, PA, USA, 1996.
17. Welding Institute Staff: 'Welding metallurgy of stainless steels: modular learning system'; 1994, Westminster, John Knox Press.
18. P. Ernst, N. J. Laycock, M. H. Moayed and R. C. Newman: *Corros. Sci.*, 1997, **39**, 1133–1136.
19. P. Muraleedharan, F. Schneider, K. Mummert: *J. Nucl. Mater.* 1999, **270**, 342–348.
20. B. T. Lu, Z. K. Chen, J. L. Luo, B. M. Patchett and Z. H. Xu: *Electrochim. Acta* 2005, **50**, 1391–1403.
21. R. Akid and D. J Mills: *Corros. Sci.*, 2001, **43**, 1203–1216.
22. M. R. Tavakoli Shoushtari, M. H. Moayed and A. Davoodi: *Corros. Eng. Sci. Technol.*, 2011, **46**, 418–427.